IEEE Access
Multidisciplinary | Rapid Review | Open Access Journal

Received April 8, 2020, accepted May 7, 2020, date of publication June 3, 2020, date of current version July 2, 2020.

Digital Object Identifier 10.1109/ACCESS.2020.2999609

Dual-Mode Wound Rotor Synchronous Machine for Variable Speed Applications

MUHAMMAD AYUB[1,5], SHAHID ATIQ[2], QASIM ALI[3], ASIF HUSSAIN[4], AND BYUNG-IL KWON[1], (Senior Member, IEEE)

[1]Department of Electrical and Electronic Engineering, Hanyang University, Ansan15588, South Korea
[2]Department of Electrical Engineering, Khwaja Fareed University of Engineering and Information Technology, Rahim Yar Khan 64200, Pakistan
[3]Department of Electrical Engineering, IBA Sukkur, Sukkur 65200, Pakistan
[4]Department of Electrical Engineering, UMT, Lahore 54770, Pakistan
[5]Department of Electronic Engineering, BUITEMS, Quetta 87300, Pakistan

Corresponding author: Byung-Il Kwon (bikwon@hanyang.ac.kr)

This work was supported in part by the Korea Institute of Energy Technology Evaluation and Planning (KETEP) and the Ministry of Trade, Industry, and Energy (MOTIE), South Korea, under Grant 20174030201780, and in part by the BK21PLUS Program through the National Research Foundation of Korea within the Ministry of Education.

ABSTRACT This paper presents a novel dual-mode wound rotor synchronous machine (DWRSM) for variable speed applications. The proposed machine combines the advantages of both the conventional wound rotor synchronous machine (CWRSM) and the brushless wound rotor synchronous machine (BWRSM). Unlike the existing BWRSM, through the dual-mode operation of the proposed machine, constant torque is achieved in the constant torque region by operating the machine in mode-I, i.e., as a CWRSM, and constant power is achieved in the field weakening region by operating the machine in mode-II, i.e., as a BWRSM. The mode change is performed through an additional thyristor drive circuit. The airgap magnetomotive force (MMF) in both modes is derived analytically. To verify this principle, finite element analysis (FEA) and an experiment on a 1- horsepower prototype machine was performed, and key influential factors were verified. The transients in the stator currents and torque during the mode change was analyzed. The test results validated the correctness of the theory and the FEA results.

INDEX TERMS Brushless, dual-mode, harmonic winding, sub-harmonic, wound rotor synchronous machine.

I. INTRODUCTION

Variable speed applications such as (hybrid) electric vehicles (EVs), compressors, pumps, blower fans, rolling mills, generators, washing machines, etc., are being developed as a means to address environmental concerns and to solve the problems associated with internal combustion engine vehicles [1]–[3]. Permanent magnet synchronous machines (PMSMs) have been used for such applications due to their high efficiency, high torque density, robust structure, and for not needing an external excitation system [4]–[7]. However, the limited supply and increasing price of permanent magnet (PM) material has significantly increased the cost of these machines [8]–[12].

The associate editor coordinating the review of this manuscript and approving it for publication was Giovanni Angiulli.

Therefore, there is a need to search for alternatives to PMSMs that require a low volume of permanent magnets such as hybrid excited synchronous machines [13]–[16] or machines that do not require permanent magnets at all, such as wound rotor synchronous machines (WRSMs) [17]. In [18], different machine topologies including those of PMSMs, induction machines (IMs), and WRSMs have been studied for EV application. In [17], [18], magnet-free electrical motors, such as IMs and WRSMs were presented as viable alternatives to rare-earth magnet motors in EV applications. However, the presence of brushes and slipring assemblies in a conventional WRSM (CWRSM) causes losses, sparking and maintenance issues. Moreover, CWRSMs require an external DC supply to provide the field current for the rotor field winding. These issues make CWRSMs less suitable for EV applications. The CWRSMs is also adopted in Renault Zoe EV due to advantages associated with it, i.e., wide speed

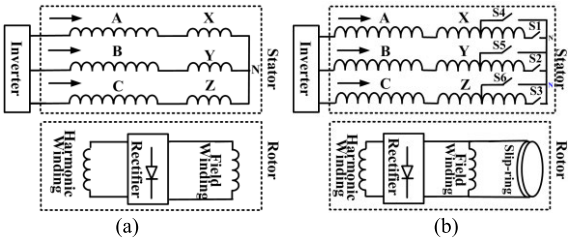

FIGURE 1. WRSM topologies. (a) Existing topology. (b) Proposed topology.

range operation with better efficiency, better flux regulation, and better over-load capability.

To overcome the issues with PM machines and WRSMs, several brushless topologies for WRSMs have been presented in recent years.

In [19]–[24], the brushless operation of a CWRSM was achieved by utilizing an additional harmonic components of stator magnetomotive force (MMF) to induce the voltage in the rotor harmonic winding. This induced voltage was then rectified, and it supplied a DC current to the rotor field winding to generate the rotor flux. The main disadvantage of these brushless wound rotor synchronous machines (BWRSMs) is the use of two inverters and extra circuitry to achieve brushless operation which increased the cost and size of the overall system.

In [25], [26], a single inverter-fed brushless topology was proposed for a WRSM in which a sub-harmonic MMF was generated by using a special stator winding arrangement, as shown in Fig. 1(a).

In the existing brushless topology of [21]–[27], the stator current was the only source of excitation, and the field current was induced from the harmonic component of the stator MMF. During the operation of the BWRSM in the constant torque region, the induced voltage in the harmonic winding varied with the variation in the speed of the machine. This resulted in a gradual increase in the field current with the increased in the speed of the machine, which resulted in a low starting torque in the constant torque region. Therefore, the torque in the constant torque region could not be maintained at a constant level by these BWRSMs. However, at or above the rated speed, these machines worked properly.

In [28], [29] a consequent-pole hybrid excited BWRSM was studied to increase the starting torque of the BWRSM. Although the starting torque of the BWRSM was increased owing to the presence of permanent magnets, the machine was not able to achieve constant torque in the constant torque region below the rated speed. This implies that these BWRSMs were only suitable for their rated speed or high speeds and were not applicable to variable speed applications.

The main purpose of this paper is to propose dual-mode operation of WRSM that is suitable for variable speed applications. The proposed dual-mode wound rotor synchronous machine (DWRSM) offers the advantages of low cost and simple field weakening control compared with PM machines. Moreover, the dual-mode operation of the proposed topology overcomes the disadvantage of inconstant torque compared with existing BWRSMs. First, the configuration of the proposed machine topology is explained. Furthermore, the operation principle of the proposed DWRSM is presented. Moreover, the airgap MMFs for both modes are derived analytically. Second, the operation principle of the proposed DWRSM is verified by the finite element analysis (FEA). Third, a prototype and its experimental analysis are presented to validate the theoretical and FEA of the proposed DWRSM. Finally, the conclusions of this work are then presented.

II. PROPOSED DUAL-MODE TOPOLOGY, OPERATION PRINCIPLE AND MACHINE CONFIGURATION

A. DUAL-MODE TOPOLOGY

Based on the existing brushless topology shown in Fig. 1(a) which has a low starting torque due to the lack of any external rotor excitation [25], the proposed DWRSM is designed to introduce a topology that can produce constant torque below the base speed when working as a CWRSM, whereas it exhibits constant power above the base speed when working as a BWRSM. Fig. 1(b) shows the proposed DWRSM topology. The three phase windings of the stator are divided into two winding sets; winding ABC and winding XYZ. Both windings are connected in series and have an equal number of turns. The end terminals of winding XYZ are joined to create a neutral point using thyristor-switch-1(S1) to S3 of the machine, and the three-phase sinusoidal currents are supplied to the stator winding through an inverter. Winding XYZ of the stator is tapped at the center point using switches S4 to S6 to achieve dual-mode operation of the proposed machine.

There are two separate windings on the rotor, i.e., the harmonic winding and the field winding. Both windings are connected through a diode bridge rectifier mounted on the rotor periphery. The harmonic winding is responsible for the induction of the voltage required for the excitation of the rotor in the brushless mode of the proposed machine. The other winding is the field winding, which is connected in parallel with the harmonic winding through the rectifier. The rotor field winding is also connected to the brushes and slipring assembly.

B. DUAL-MODE OPERATION PRINCIPLE

There are two modes of operation of the proposed DWRSM topology i.e. mode-I and mode-II which are shown in Fig. 2(a) and (b), respectively.

1) MODE-I FOR CONSTANT TORQUE OPERATION

The configuration for mode-I of the proposed topology is shown in Fig. 2(a). In this mode, the switches S1 to S3 are in the ON state and S4 to S6 are in the OFF state. The three phase sinusoidal currents are supplied to the stator winding through the inverter. The field winding is connected to the external DC supply through the brushes and slip ring assembly.

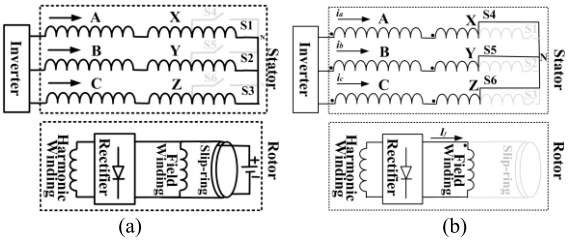

FIGURE 2. Proposed dual-mode topology. (a) Mode-I. (b) Mode-II.

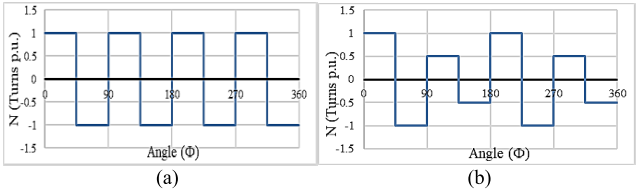

FIGURE 3. Phase A winding function. (a) Mode-I. (b) Mode-II.

The generation of the airgap MMF in mode-I is theoretically explained by considering an eight-pole machine with concentrated full pitch winding on the stator. For mode-I operation of the DWRSM, the three phase alternating currents (ACs) excite the stator windings and generate the rotating MMF. The rotating MMF can be expressed as

$$F(\emptyset, i) = \sum_{i=1}^{m} N_i(\emptyset)\, i_i(t) \tag{1}$$

where $\emptyset$ denotes the angular measure around the airgap of the machine, $N_i(\emptyset)$ is the winding function describing the position and the polarity of the coil sides, and $i_i(t)$ is the current in the respective winding. The MMF for the three phase windings can be expressed as

$$F_{ABC}(\emptyset, i) = N_A(\emptyset)\, i_A(t) + N_B(\emptyset)\, i_B(t) + N_C(\emptyset)\, i_C(t) \tag{2}$$

Conventionally, the three phase currents are balanced and 120° out of phase with each other. Also, the winding function of each phase winding is displaced by 120° with respect to $\emptyset$. This results in a rotating MMF in the conventional machine. For the supposed full pitched concentrated winding, the three winding functions for the three phases become rectangular waves. Fig. 3(a) shows the rectangular winding function for phase A in mode-I. The rectangular wave winding functions can be expressed as a Fourier series of odd harmonics. The winding functions for phases A, B, and C can be represented as

$$N_A(\emptyset) = \frac{4N}{\pi}\left(\sin\emptyset + \frac{1}{3}\sin 3\emptyset\right) \tag{3}$$

$$N_B(\emptyset) = \frac{4N}{\pi}\left(\sin\left(\emptyset - \frac{2\pi}{3}\right) + \frac{1}{3}\sin 3\emptyset\right) \tag{4}$$

$$N_C(\emptyset) = \frac{4N}{\pi}\left(\sin\left(\emptyset + \frac{2\pi}{3}\right) + \frac{1}{3}\sin 3\emptyset\right) \tag{5}$$

The three phase windings are excited by three phase armature currents, which can be represented as

$$i_A(t) = I_1 \sin\omega t \tag{6}$$

$$i_B(t) = I_1 \sin\left(\omega t - \frac{2\pi}{3}\right) \tag{7}$$

$$i_C(t) = I_1 \sin\left(\omega t + \frac{2\pi}{3}\right) \tag{8}$$

Utilizing the expressions for winding functions and currents, the MMF can be written as

$$\begin{aligned} F_{ABC}(\emptyset, i) = {} & \frac{4}{\pi}NI_1\left\{\sin\emptyset\sin\omega t + \sin\left(\emptyset - \frac{2\pi}{3}\right)\sin\left(\omega t - \frac{2\pi}{3}\right)\right. \\ & \left. + \sin\left(\emptyset + \frac{2\pi}{3}\right)\sin\left(\omega t + \frac{2\pi}{3}\right)\right\} \\ & + \frac{4}{\pi}NI_1\left\{\frac{1}{3}sin3\emptyset\left(\sin\omega t + \sin\left(\omega t - \frac{2\pi}{3}\right)\right.\right. \\ & \left.\left. + \sin\left(\omega t + \frac{2\pi}{3}\right)\right)\right\} \end{aligned} \tag{9}$$

The second term in equation (9) becomes zero because the sum of three balanced sine waves is zero. Thus

$$\begin{aligned} F_{ABC}(\emptyset, i) = {} & \frac{4}{\pi}NI_1\left\{\sin\emptyset\sin\omega t + \sin\left(\emptyset - \frac{2\pi}{3}\right)\sin\left(\omega t - \frac{2\pi}{3}\right)\right. \\ & \left. + \sin\left(\emptyset + \frac{2\pi}{3}\right)\sin\left(\omega t + \frac{2\pi}{3}\right)\right\} \end{aligned} \tag{10}$$

As shown in (10), the machine airgap has dominant fundamental MMF component if higher order harmonics (i.e., 5^{th}, 7^{th}, etc.) are ignored. Therefore, the proposed DWRSM works as a CWRSM in this mode.

2) MODE-II OF THE CONSTANT POWER OPERATION

The configuration of mode-II of the proposed DWRSM topology is shown in Fig. 2(b). In this mode, the proposed topology works as a BWRSM. The switches S1 to S3 are OFF, and S4 to S6 are now ON to tap winding XYZ of each stator at the center point, such that the number of turns in winding XYZ becomes half than that of winding ABC.

Meanwhile, the field winding is disconnected from the external DC supply. The advantages by creating difference in the number of turns in both windings, winding ABC and winding XYZ, are twofold, primarily, the difference between winding ABC and XYZ turns is responsible for the generation of a sub-harmonic MMF alongside fundamental MMF; secondary, it decreases the stator total number of turns per phase by a factor of 4, which will consequently help to increase the constant power speed region.

The generation of the airgap MMF having a sub-harmonic MMF along with the fundamental component is derived in this section.

Due to difference in the number of turns of ABC and XYZ windings, if higher order harmonics are ignored, the winding

functions in this mode for phases A, B, and C can be represented as

$$N_A(\emptyset) = \frac{2N}{\pi}\left(\sin\emptyset + \frac{1}{3}sin3\emptyset\right) + \frac{N}{\pi}\left(\cos\left(\frac{\emptyset}{2}\right) + sin\emptyset\right) \tag{11}$$

$$N_B(\emptyset) = \frac{2N}{\pi}\left(\sin\left(\emptyset - \frac{2\pi}{3}\right) + \frac{1}{3}sin3\emptyset\right) + \frac{N}{\pi}\left(\cos\left(\frac{\emptyset - \frac{2\pi}{3}}{2}\right) + sin\left(\emptyset - \frac{2\pi}{3}\right)\right) \tag{12}$$

$$N_c(\emptyset) = \frac{2N}{\pi}\left(\sin\left(\emptyset + \frac{2\pi}{3}\right) + \frac{1}{3}sin3\emptyset\right) + \frac{N}{\pi}\left(\cos\left(\frac{\emptyset + \frac{2\pi}{3}}{2}\right) + sin\left(\emptyset + \frac{2\pi}{3}\right)\right) \tag{13}$$

Fig. 3(b) shows the winding function for phase A in mode-II. The input currents for mode-II are the same three-phase sinusoidal currents as for the CWRSM (mode-I). The airgap MMF, ignoring higher order harmonics (i.e., 5^{th}, 7^{th}, etc.). in mode-II can be represented as,

$$\begin{aligned} F_{ABC}(\emptyset, i) &= \frac{3}{\pi}NI_1\left\{\sin\emptyset\sin\omega t + \sin\left(\emptyset - \frac{2\pi}{3}\right)\sin\left(\omega t - \frac{2\pi}{3}\right) + \sin\left(\emptyset + \frac{2\pi}{3}\right)\sin\left(\omega t + \frac{2\pi}{3}\right)\right\} \\ &+ \frac{1}{\pi}NI_1\left\{\cos\left(\frac{\emptyset}{2}\right)\sin\omega t + \cos\left(\frac{\emptyset - \frac{2\pi}{3}}{2}\right)\sin\left(\omega t - \frac{2\pi}{3}\right) + \cos\left(\frac{\emptyset + \frac{2\pi}{3}}{2}\right)\sin\left(\omega t + \frac{2\pi}{3}\right)\right\} \end{aligned} \tag{14}$$

The second term in equation (14) is the sub-harmonic MMF term in the airgap MMF, which is responsible for the brushless excitation of the rotor in mode-II.

This sub-harmonic MMF induces the voltages in the same pole-pair rotor harmonic winding, which is then rectified by the rotating rectifier mounted on the rotor periphery, and a DC current to the field winding of the machine is supplied. In mode-II, the stator current is the only source of excitation. Part of this current is utilized to generate the sub-harmonic component for the brushless excitation and the rest of the stator current is used for torque production. The proposed DWRSM is operated in the constant power region by a field weakening control using negative d-axis stator currents.

C. PROPOSED MACHINE CONFIGURATION

The proposed DWRSM is verified by designing an eight-pole, twelve-slot machine with the three-phase double layer distributed windings on the stator. The machine layout with the stator and rotor winding configuration is shown in Fig. 4. To realize the operation of the proposed DWRSM, the stator winding is distributed in such a way that winding ABC and winding XYZ are placed on alternate portions of the machine and are connected in series with each other.

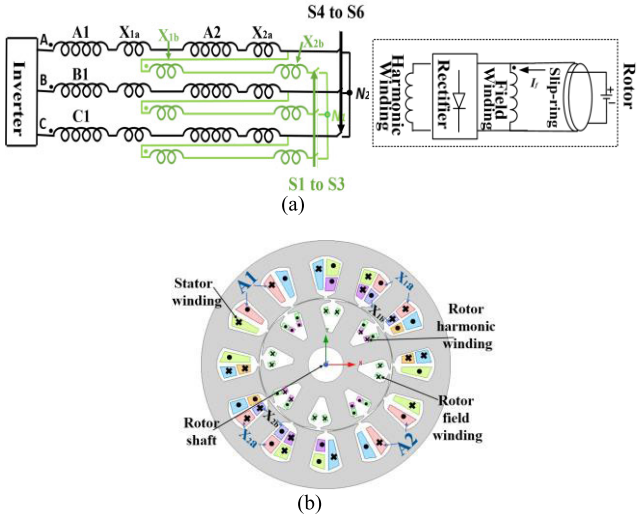

FIGURE 4. Proposed DWRSM (a) Winding configuration. (b) Machine layout with stator and rotor winding configuration.

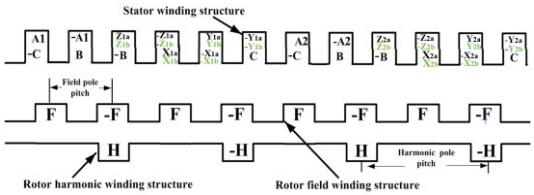

FIGURE 5. Stator and rotor winding structure.

There are two separate windings on the rotor of the machine: the harmonic winding and the field winding. To realize the operating principle of the proposed topology, the pole pitch of the rotor harmonic winding is kept double that of the pole pitch of the rotor field winding. Consequently, the harmonic winding has four-pole. The field winding has eight-poles and is used to synchronize with the eight-pole stator MMF to generate output torque. The structure of the stator and rotor windings is shown in Fig. 5. The machine parameters of the designed DWRSM are summarized in Table 1.

III. DECOUPLING ANALYSIS BETWEEN ROTOR HARMONIC AND STAROR WINDING

There is an extra winding on the machine rotor, i.e., the harmonic winding, therefore, to check the magnetic decoupling between the rotor harmonic winding and the stator winding and vice versa, the following analysis was performed [30], [31]. To verify the decoupling between the two windings, a fictitious eight-pole stator (only phase-1) and four-pole rotor harmonic winding was considered, and it is shown in Fig. 6. The electromagnetic decoupling of the two flux components was derived.

In the figure, the stator coil pitch is 45° degrees, while the rotor harmonic coil pitch is 90° degrees. The difference between the stator coil and rotor coil is 45° degrees, hence the flux linkages of the stator coils in phase-1 due to the rotor

TABLE 1. Machine design parameters.

Parameter	Units	Proposed DWRSM	
		mode-I	mode-II
Rated power	W	746	
Rated speed	rpm	900	
Stator outer diameter	mm	177	
Stator inner diameter	mm	95	
Air gap length	mm	0.5	
Stack length	mm	80	
Shaft diameter	mm	25	
Number of poles	-	8	
Number of stator slots	-	12	
Winding ABC/XYZ turns per phase	-	160/160	160/80
Field/harmonic winding turns	-	224/-	224/32
Core material	-	50H1300	

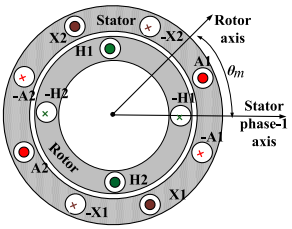

FIGURE 6. Fictitious machine for decoupling analysis.

harmonic flux are given by

$$\begin{aligned}
\lambda_{A_1,-A_1} &= k_w N_{ph}\phi_p \cos\left(\frac{(\pi/4)}{2}\right)\cos(\theta_m)\\
\lambda_{X_1,-X_1} &= k_w N_{ph}\phi_p \cos\left(\frac{(\pi/4)}{2}\right)\cos\left(\theta_m-\frac{\pi}{2}\right)\\
\lambda_{A_2,-A_2} &= k_w N_{ph}\phi_p \cos\left(\frac{(\pi/4)}{2}\right)\cos(\theta_m-\pi)\\
\lambda_{X_2,-X_2} &= k_w N_{ph}\phi_p \cos\left(\frac{(\pi/4)}{2}\right)\cos\left(\theta_m-\frac{3\pi}{2}\right) \qquad (15)
\end{aligned}$$

From (15), the induced EMFs in each stator coil are calculated as

$$\begin{aligned}
e_{A_1,-A_1} &= -\omega_m k_w N_{ph}\phi_p \cos\left(\frac{(\pi/4)}{2}\right)\sin(\omega_m t)\\
e_{X_1,-X_1} &= -\omega_m k_w N_{ph}\phi_p \cos\left(\frac{(\pi/4)}{2}\right)\sin\left(\omega_m t-\frac{\pi}{2}\right)\\
e_{A_2,-A_2} &= -\omega_m k_w N_{ph}\phi_p \cos\left(\frac{(\pi/4)}{2}\right)\sin(\omega_m t-\pi)\\
e_{X_2,-X_2} &= -\omega_m k_w N_{ph}\phi_p \cos\left(\frac{(\pi/4)}{2}\right)\sin\left(\omega_m t-\frac{3\pi}{2}\right) \qquad (16)
\end{aligned}$$

where $\theta_m = \omega_m t$.

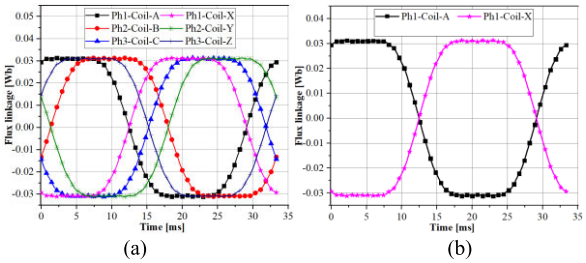

FIGURE 7. Flux linkage due to rotor harmonic winding flux. (a) All stator coils; (b) phase-1 coils.

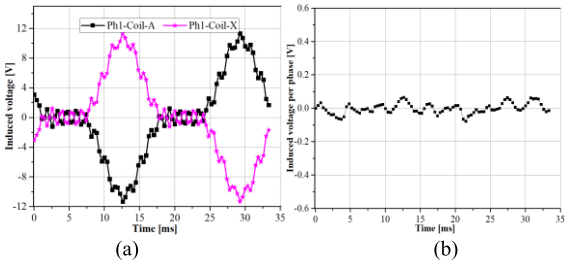

FIGURE 8. Induced voltage due to rotor harmonic winding flux. (a) phase-1 coils, separately; (b) phase-1 coils, sum.

Therefore, the total induced EMF in the series-wound coils of phase-1 is

$$e_{A_1,-A_1} + e_{X_1,-X_1} + e_{A_2,-A_2} + e_{X_2,-X_2} = 0 \qquad (17)$$

Equation (17) shows there is no mutual coupling between the rotor harmonic winding and stator winding. To verify the decoupling FEA is performed. A 5 A dc current is applied to the rotor harmonic winding, whereas, the stator winding coils are kept open. The flux linkage on the individual stator coils is shown in Fig. 7(a), and the flux linkage for phase-1 coils only is given in Fig. 7(b). The flux in the coils of phase-1 clearly shows that both coils, coil-A and coil-X, have flux linkages that are 180° degrees out of phase. The induced voltage in the coils of phase-1 is shown in Fig. 8(a). The overall induced voltage in phase-1 is shown in Fig. 8(b) and is less than 0.1 volts in this case. Thus, the simulation results verify that the rotor harmonic winding and stator winding, and vice versa, are mutually decoupled, and do not present interference to each other.

IV. ANALYTICAL PERFORMANCE ANALYSIS BY 2-D FINITE ELEMENT METHOD (FEM)

A 2-D FEM was utilized to demonstrate the operation principle and effectiveness of the proposed DWRSM. The proposed machine was analyzed in both modes; mode-I and mode-II.

A. NO-LOAD ANALYSIS OF DWRSM IN MODE-I AT RATED SPEED

The proposed DWRSM was analyzed by supplying a DC field current of 9.3 A dc to the rotor field winding of the machine. The stator and rotor winding structure of the proposed machine were kept as shown in Fig. 5. The no-load

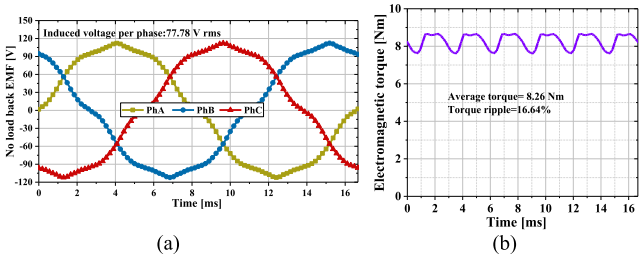

FIGURE 9. Mode-I (a) No-load back EMF. (b) Load electromagnetic torque.

analysis was carried out at the rated speed of 900 rpm. The resulting back EMF is shown in Fig. 9(a). The induced voltages for the three phases are balanced and have 77.78 V rms per phase.

B. LOAD ANALYSIS OF DWRSM IN MODE-I AT RATED SPEED

The proposed DWRSM is analyzed at the rated load of 1-hp by supplying a three-phase sinusoidal current of 3.5 A rms at a frequency of 60 Hz to the stator winding, and the field current was kept at 9.3 A dc. Fig. 9(b) shows the torque of the proposed DWRSM during mode-I operation. An average torque of 8.26 Nm with a torque ripple of 16.64% was observed at the rated speed of 900 rpm.

Fig. 10(a) shows the flux density distribution in the rated load condition in mode-I of the proposed DWRSM. The flux density plot shows balanced distribution, because both stator windings have an equal number of turns due to the mode-I operation of the proposed machine.

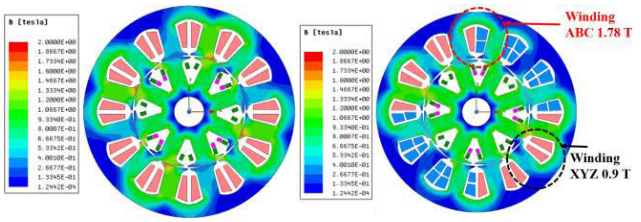

FIGURE 10. DWRSM (a) Mode-I: flux density distribution. (b) Mode-II: flux density distribution.

C. LOAD ANALYSIS OF DWRSM IN MODE-II AT RATED SPEED

The FEM analysis of the proposed DWRSM was carried out in mode-II. To operate the proposed machine in mode-II as given in Fig. 2(b), a three-phase current of 4.5 A rms at a frequency of 60 Hz was supplied to the stator winding. Due to mode-II (BWRSM) operation, the rotor field winding was disconnected from the DC exciter.

The flux density distribution of the proposed DWRSM in mode-II operation at the rated load is shown in Fig. 10(b). Due to the special arrangement of the stator winding, the number of turns of winding XYZ are kept to half that of winding ABC. Owing to the different number of turns, the flux density distribution is not uniform in the stator of the machine. The maximum flux density in the portions of stator with winding ABC is approximately 1.78 T, whereas, the maximum flux density in the portions of the stator with winding XYZ is 0.9 T. This difference in flux density distribution was responsible for the generation of the sub-harmonic MMF along with the fundamental component of the stator MMF.

The airgap flux density plot is shown in Fig. 11(a). The difference in the peak values of the airgap flux density is due to the special winding arrangement used for the proposed brushless topology. The harmonic order of the normalized flux density is shown in Fig. 11(b). It demonstrates the two-pole pairs of the sub-harmonic component of the stator MMF, and the four-pole pairs of the fundamental component of the stator MMF.

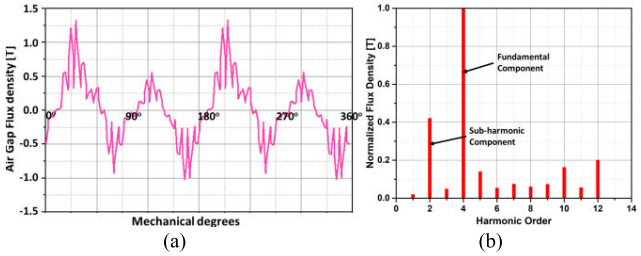

FIGURE 11. (a) Airgap flux density. (b) Harmonic order of the flux density.

The sub-harmonic component of the stator MMF induces alternating voltage in the rotor harmonic winding. The induced voltage is rectified through the rotary rectifier mounted on the rotor and DC current is provided to the field winding of the machine. Fig. 12(a) shows the induced AC in the rotor harmonic winding and the rectified field current. It can be observed that after rectification, the harmonic winding voltage is able to establish a stable excitation current in the field winding, which confirms the feasibility of mode-II operation of the proposed DWRSM.

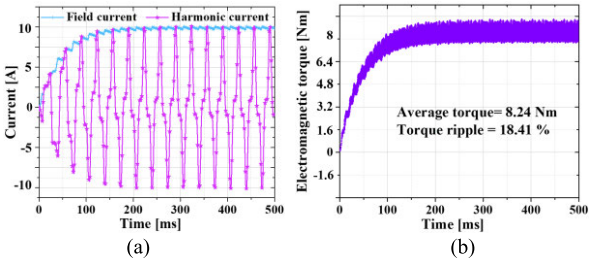

FIGURE 12. Machine performance at rated load condition for mode-II. (a) Rotor currents. (b) Electromagnetic torque.

Fig. 12(b) shows the electromagnetic torque of mode-II operation of the proposed DWRSM. An average torque of 8.24 Nm with a torque ripple of 18.41% is observed in this mode. The difference in the torque and torque ripple compared with mode-I operation is due to the brushless operation of the proposed DWRSM.

D. WIDE SPEED-RANGE OF CWRSM, BWRSM, AND DWRSM

The electromagnetic performance of the proposed DWRSM was compared with a CWRSM and a BWRSM by 2-D FEA. Three machine models were analyzed over a wide speed range.

The voltage and current constraints are given in Table 2 for all three machines and a negative d-axis field weakening control is adopted for operation over a wide speed range.

TABLE 2. Current and voltage constraints.

Mode of operation	Voltage constraint	Field currents (A dc)	Armature currents (A rms)	Control technique
CWRSM	120 V rms	9.3	3.5	Negative d-axis
BWRSM		0	4.5	
DWRSM		9.3/0	3.5/4.5	

For CWRSM, the torque, power and efficiency curves with respect to rotor speed are given in Fig. 13(a).

In Fig. 13(a), constant torque is maintained up to the rated speed of 900 rpm. Beyond the rated speed, a negative d-axis flux weakening control is adopted, and the machine is analyzed up to 3500 rpm in a wide speed region. The efficiency on some critical points on the torque speed curve is also plotted. The efficiency is maintained around 81% near the rated speed and it drops to around 76% with wider speed due to increased core losses. Power starts to drop after 2700 rpm in this mode.

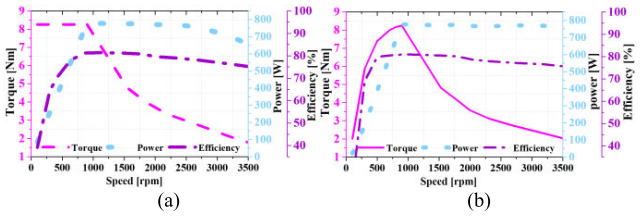

FIGURE 13. Torque power and efficiency curves. (a) CWRSM. (b) BWRSM.

For BWRSM, the torque, power, and efficiency curves with respect to rotor speed are shown in Fig. 13(b).

The power is maintained at a constant until 3500 rpm. Efficiency is approximately 80% at the rated speed and drops to 75.15% around 3500 rpm. The torque is not maintained in the constant torque region (below rated speed) due to the absence of a initial rotor flux in the brushless operation. This torque behavior, and the zero starting torque are considered major drawback in BWRSM topologies. The speed range is increased due to the decrease in stator turns in this mode.

For DWRSM, the torque, power, and efficiency curves, with respect to rotor speed are shown in Fig. 14.

To maintain the constant torque region and high starting torque, the machine was analyzed as a CWRSM with a 9.3 A dc field current and 3.5 A rms per phase armature currents as given in Table 2 initially (i.e., mode-I), and after the rated speed was achieved, the machine was switched to the BWRSM operation and kept in that mode throughout the constant power region (mode-II).

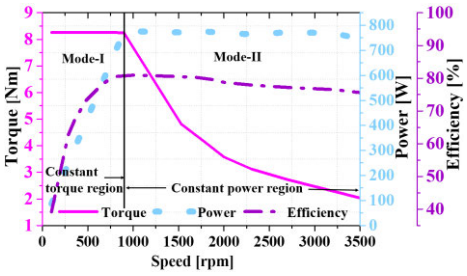

FIGURE 14. Torque power and efficiency curves of DWRSM.

TABLE 3. Three machine comparison.

Mode of operation	Torque at and below rated speed [Nm]	Power at and above rated speed	Starting torque [Nm]	Stator winding fill factor	
				ABC	XYZ
CWRSM	8.26	~ 778 W	8.26	40%	40%
BWRSM	0 ~ 8.24	~ 777 W	0	40%	20%
DWRSM	8.26	~ 778 W	8.26	40%	40%

The overall comparison of all three machines is given in Table 3. It shows that the proposed DWRSM maintained constant torque and constant power regions. The starting torque and asymmetry fill factors issues are also removed previously associated with BWRSM topology. Compared with CWRSM, the proposed DWRSM has following advantages,

- A wider constant power speed region.
- Less frequent brush and slipring maintenance required, as the electrical stress on the brushes and slipring is removed in the constant power region.
- No losses associated with brushes, sliprings, or field exciter in the constant power region.
- No sparking occurring between the brushes and slipring assembly in the constant power region.

The disadvantages of the proposed DWRSM compared to CWRSM are,

- Extra rotor harmonic winding copper losses, which in this case was less than 1% of the output power in the constant power region, and
- An additional six thyristor switches for mode change on the stator winding side.

V. EXPERIMENT VERIFICATION OF THE PROPOSED DWRSM

A prototype machine was manufactured to verify the operation of the proposed DWRSM. The stator, rotor and assembled prototype are shown in Fig. 15 (a), (b), and (c), respectively, and the experimental setup is given in Fig. 16. The stator winding was wound so that the XYZ winding sets were divided into two portions, as discussed in Section II, and as shown in Fig. 15 (c) and 16.

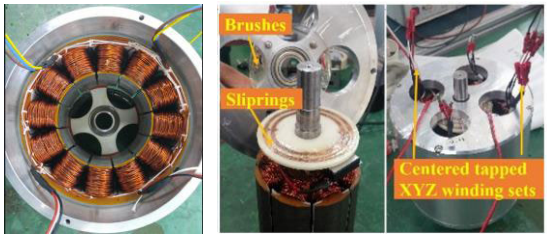

FIGURE 15. Prototype Machine. (a) Stator. (b) Rotor. (c) Assembled Prototype.

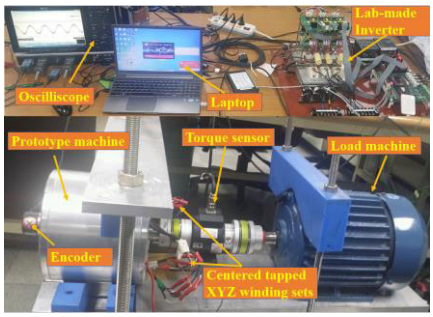

FIGURE 16. Experimental Setup.

A. NO-LOAD ANALYSIS OF DWRSM IN MODE-I AT RATED SPEED

For the no-load experimental analysis in mode-I, the field winding of the rotor is supplied with a 9.3 A dc current, and the prototype was rotated by a prime mover at the rated speed of 900 rpm. A balanced no-load back EMF was induced with 76.5 V rms in each phase. The no-load back EMF is shown in Fig. 17.

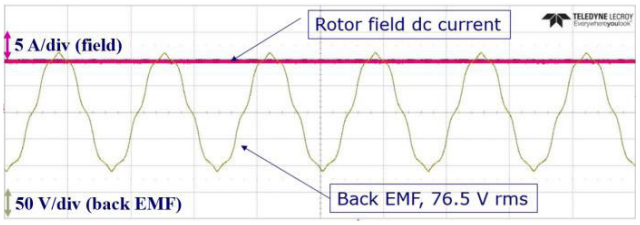

FIGURE 17. No-load back-EMF in mode-I at rated speed of 900 rpm.

B. LOAD ANALYSIS OF DWRSM IN MODE-I AT RATED SPEED

For the load analysis in mode-I, the machine stator was supplied with the rated currents of 3.5 A rms at a frequency of 60 Hz, whereas, a 9.3 A dc current was supplied to the rotor field winding. The experimental output torque of the prototype at the rated speed of 900 rpm is given in Fig. 18, where, the average torque is **8.221 Nm,** with a **torque ripple of 18.72%.** One phase of the stator current and DC field current is also shown in the figure.

C. LOAD ANALYSIS OF DWRSM IN MODE-II AT RATED SPEED

For load analysis in mode-II, Fig. 2(b), as a BWRSM, the XYZ winding set was switched to centrally tapped terminals, as shown in Fig. 2(b). the rotor field winding was disconnected from the brushes and slipring. the stator of the machine was supplied with a rated current of 4.5 A rms at 60 Hz frequency. The centrally tapped winding arrangement of the XYZ winding set was able to generate an airgap MMF containing a sub-harmonic component alongside the fundamental harmonic as per the theory presented in Section II (B). The sub-harmonic component (i.e. four-pole in this case) was collected by an equal number of poles of rotor harmonic winding. After rectification, the rotor field winding current was successfully built, and the torque was achieved. The rotor induced field current is given in Fig. 19 has an 8.89 A dc stable value. The output torque and phase currents are also shown in the figure. The identical torques of the FEA and prototype verified the brushless operation of the proposed DWRSM at rated speed. The average torque in mode-II was 8.21 Nm with a torque ripple of **20.3%.** The stable three phase currents with few high value currents i.e., 4.65 A rms compared with the FEA currents, i.e., 4.5 A rms, are also shown.

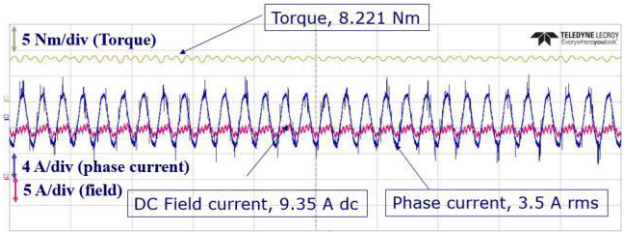

FIGURE 18. Output Torque and phase currents in mode-I @900 rpm.

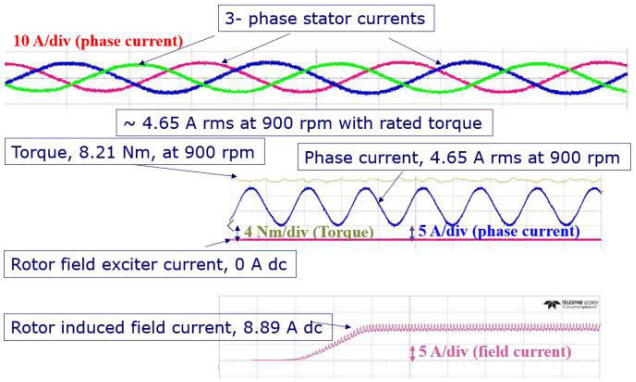

FIGURE 19. Output Torque, phase currents, and rotor induced field current in mode-II 900rpm.

D. TRANSIENT ANALYSIS DURING MODE CHANGE

The phase currents, DC field current, and output torque were observed during the mode change. The winding mode change was performed in two steps to lower the transients in the phase currents and output torque. The machine was started as a CWRSM (mode-I), where the rotor field winding was supplied with a 9.3 A dc current and 3.5 A rms per phase was supplied to the stator winding. S1 to S3 of the stator winding were in the closed state, and S4 to S6 were in the open state. After the rated speed was achieved in mode-I,

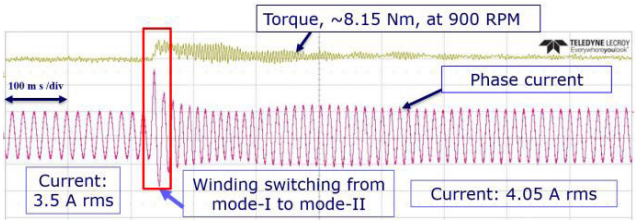

FIGURE 20. Transient analysis step-1: Torque and phase currents before, during, and after winding switching.

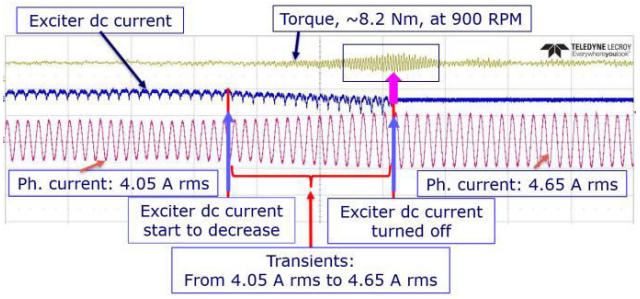

FIGURE 21. Transient analysis step-2: Torque and phase currents at rated field current, decreasing field current, and zero field current.

the machine was switched to the BWRSM (mode-II). The mode conversion was performed in two steps.

Initially, in step-1, the thyristor switches S4 to S6 were triggered with a closed gate signal first, and then the S1 to S3 switches were triggered from ON to OFF. During the switching, S4 to S6 were first switched from OFF to ON, and then S1 to S3 were switched from ON to OFF. The transient results were measured and are shown in Fig. 20. The phase current and output torque are also shown. S1 to S3 were connected during the switching, therefore the stator current showed continuity. At the instant of S4 to S6 switching, approximately twice the rated current flowed for one cycle. The instantaneous response can also be verified in the output torque shape, where a slight increase in the output torque can be observed. After S4 to S6 were triggered, the phase current showed turmoil due to circulating currents in the X coils. Nonetheless, the circulating currents vanished, and the phase currents got stabilized with the switching off of S1 to S3. The stator phase current in this step was increased from 3.5 A rms to 4.05 A rms.

In step-2, the DC rotor field current was decreased gradually. The DC rotor field, the stator current, and the output torque during step-2 is shown in Fig. 21. The phase current increased from 4.05 A rms to 4.65 A rms with the gradual decrease in the rotor excitor DC current. A slight torque ripple was observed when the exciter DC current was completely disconnected from the rotor field winding.

E. TORQUE SPEED CHARACTERISTICS OF THE PROPOSED DWRSM

The prototype was experimentally analyzed for wide speed range operation. In the constant torque region, the machine

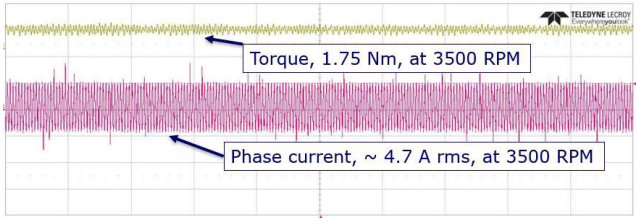

FIGURE 22. Torque and phase current at 3500 rpm.

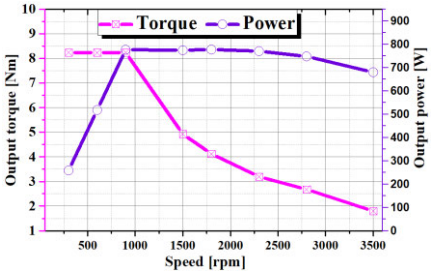

FIGURE 23. Torque speed curve of the proposed DWRSM.

TABLE 4. FEA and experimental results comparison.

Mode of operation	Units	DWRSM	
		FEA	Experiment
No-load back EMF	V rms	77.78	76.50
Torque in mode-I at 900 rpm	Nm	8.26	8.221
Torque ripple in mode-I	%	16.64	18.72
Torque in mode-II at 900 rpm	Nm	8.24	8.21
Torque ripple in mode-II	%	18.41	20.3

was tested in mode-I, which is a CWRSM mode. The prototype was analyzed up to the rated speed of 900 rpm. Beyond the rated speed of 900 rpm, the machine was analyzed in mode-II, which is a BWRSM mode. In mode-II, a negative d-axis control technique was used to extend the speed beyond the rated speed under the voltage constraint of 120 V rms. The machine was operated at the maximum speed of 3500 rpm in mode-II and the resulting output torque and phase currents are shown in Fig. 22. Some critical points of average torque and output power were examined through experimentation on the prototype machine. The torque, power, and speed curves resulting from experimentation are shown in Fig. 23.

The FEA and experimental results comparison is given in Table 4. The results for the no-load and loaded analysis in both modes at the rated speed of 900 rpm show good agreement between the FEA and the experimental results, which validates the proposed DWRSM.

VI. CONCLUSION

This paper has presented a novel DWRSM for variable speed applications. Due to the dual-mode operation, the proposed machine overcomes the problem of achieving the desired torque in the constant torque region, which makes this machine topology suitable for variable speed applications.

Although brushes and sliprings are still utilized in the constant torque region in the proposed DWRSM, however, the electrical stress on the brushes and sliprings, and electrical losses of the brushes and sliprings are removed in the constant power region. Furthermore, the proposed DWRSM was analyzed for wide speed range operation, which resulted in a wide speed range of four times the rated speed. The dual-mode operation of the proposed machine was also verified by manufacturing a prototype. The mode change was performed in two steps using a thyristor drive circuit. The increase in the phase current in the transient was around two times the rated current for a duration of one cycle. The experimental results proved the feasibility of the proposed machine for variable speed applications.

REFERENCES

[1] M. Ehsani, K. M. Rahman, and H. A. Toliyat, "Propulsion system design of electric and hybrid vehicles," *IEEE Trans. Ind. Electron.*, vol. 44, no. 1, pp. 19–27, Feb. 1997.

[2] G. da Cunha, A. J. Rossa, J. A. Alves, and E. Cardoso, "Control of permanent magnet synchronous machines for subsea applications," *IEEE Trans. Ind. Appl.*, vol. 54, no. 2, pp. 1899–1905, Mar. 2018.

[3] J. Kim, K. Ha, and R. Krishnan, "Single-controllable-switch-based switched reluctance motor drive for low cost, variable-speed applications," *IEEE Trans. Power Electron.*, vol. 27, no. 1, pp. 379–387, Jan. 2012.

[4] T. A. Burress and S. L. Campbell, "Evaluation of the 2010 Toyota prius hybrid synergy drive system," Oak Ridge Nat. Lab., Oak Ridge, TN, USA, Tech. Rep. ORNL/TM-2010/253, Mar. 2011.

[5] K. T. Chau, C. C. Chan, and C. Liu, "Overview of permanent-magnet brushless drives for electric and hybrid electric vehicles," *IEEE Trans. Ind. Electron.*, vol. 55, no. 6, pp. 2246–2257, Jun. 2008.

[6] L. Dang, N. Bernard, N. Bracikowski, and G. Berthiau, "Design optimization with flux weakening of high-speed PMSM for electrical vehicle considering the driving cycle," *IEEE Trans. Ind. Electron.*, vol. 64, no. 12, pp. 9834–9843, Dec. 2017.

[7] C. C. Chan, K. T. Chau, J. Z. Jiang, W. Xia, M. Zhu, and R. Zhang, "Novel permanent magnet motor drives for electric vehicles," *IEEE Trans. Ind. Electron.*, vol. 43, no. 2, pp. 331–339, Apr. 1996.

[8] M. Barcaro and N. Bianchi, "Interior PM machines using ferrite to replace rare-Earth surface PM machines," *IEEE Trans. Ind. Appl.*, vol. 50, no. 2, pp. 979–985, Mar. 2014.

[9] N. Bianchi, S. Bolognani, and B. J. Chalmers, "Salient-rotor PM synchronous motors for an extended flux-weakening operation range," *IEEE Trans. Ind. Appl.*, vol. 36, no. 4, pp. 1118–1125, 2000.

[10] W. L. Soong and N. Ertugrul, "Field-weakening performance of interior permanent-magnet motors," *IEEE Trans. Ind. Appl.*, vol. 38, no. 5, pp. 1251–1258, Sep. 2002.

[11] R. F. Schiferl and T. A. Lipo, "Power capability of salient pole permanent magnet synchronous motors in variable speed drive applications," *IEEE Trans. Ind. Appl.*, vol. 26, no. 1, pp. 115–123, Jan./Feb. 1990.

[12] A. M. EL-Refaie and T. M. Jahns, "Optimal flux weakening in surface PM machines using fractional-slot concentrated windings," *IEEE Trans. Ind. Appl.*, vol. 41, no. 3, pp. 790–800, May 2005.

[13] M. Barcaro, N. Bianchi, and F. Magnussen, "Permanent-magnet optimization in permanent-magnet-assisted synchronous reluctance motor for a wide constant-power speed range," *IEEE Trans. Ind. Electron.*, vol. 59, no. 6, pp. 2495–2502, Jun. 2012.

[14] P. Guglielmi, B. Boazzo, E. Armando, G. Pellegrino, and A. Vagati, "Permanent-magnet minimization in PM-assisted synchronous reluctance motors for wide speed range," *IEEE Trans. Ind. Appl.*, vol. 49, no. 1, pp. 31–41, Jan. 2013.

[15] Y. Amara, L. Vido, M. Gabsi, E. Hoang, A. H. Ben Ahmed, and M. Lecrivain, "Hybrid excitation synchronous machines: Energy-efficient solution for vehicles propulsion," *IEEE Trans. Veh. Technol.*, vol. 58, no. 5, pp. 2137–2149, Jun. 2009.

[16] Z. Shushu, L. Chuang, N. Yinhang, and T. Jie, "A two-stage brushless excitation method for hybrid excitation synchronous generator," *IEEE Trans. Magn.*, vol. 51, no. 6, pp. 1–11, Jun. 2015.

[17] T. A. Lipo and Z. S. Du, "Synchronous motor drives—A forgotten option," in *Proc. Int. Aegean Conf. Electr. Mach. Power Electron. (ACEMP), Int. Conf. Optim. Electr. Electron. Equip. (OPTIM) Int. Symp. Adv. Electromech. Motion Syst. (ELECTROMOTION)*, Side, Turkey, Sep. 2015, pp. 1–5.

[18] M. Popescu, J. Goss, D. A. Staton, D. Hawkins, A. Boglietti, and Y. C. Chong, "Electrical vehicles—Practical solutions for power traction motor systems," *IEEE Trans. Ind. Appl.*, vol. 54, no. 3, pp. 2751–2762, May/Jun. 2016.

[19] I. R. Smith and P. A. Nisar, "Brushless and self-excited 3-phase synchronous machine," *Proc. Inst. Electr. Eng.*, vol. 115, no. 11, pp. 1655–1660, 1968.

[20] K. Inoue, H. Yamashita, E. Nakamae, and T. Fujikawa, "A brushless self-exciting three-phase synchronous generator utilizing the 5th-space harmonic component of magneto motive force through armature currents," *IEEE Trans. Energy Convers.*, vol. 7, no. 3, pp. 517–524, Sep. 1992.

[21] F. Yao, Q. An, X. Gao, L. Sun, and T. A. Lipo, "Principle of operation and performance of a synchronous machine employing a new harmonic excitation scheme," *IEEE Trans. Ind. Appl.*, vol. 51, no. 5, pp. 3890–3898, Sep./Oct. 2015.

[22] F. Yao, Q. An, L. Sun, and T. A. Lipo, "Performance investigation of a brushless synchronous machine with additional harmonic field windings," *IEEE Trans. Ind. Electron.*, vol. 63, no. 11, pp. 6756–6766, Nov. 2016.

[23] G. Jawad, Q. Ali, T. A. Lipo, and B.-I. Kwon, "Novel brushless wound rotor synchronous machine with zero-sequence third-harmonic field excitation," *IEEE Trans. Magn.*, vol. 52, no. 7, pp. 1–4, Jul. 2016.

[24] Q. Ali, T. A. Lipo, and B.-I. Kwon, "Design and analysis of a novel brushless wound rotor synchronous machine," *IEEE Trans. Magn.*, vol. 51, no. 11, pp. 1–4, Nov. 2015.

[25] H. Asif and B. I. Kwon, "A new brushless wound rotor synchronous machine using a special stator winding arrangement," *Elect. Eng.*, vol. 100, pp. 1797–1804, Nov. 2017.

[26] A. Hussain, S. Atiq, and B.-I. Kwon, "Optimal design and experimental verification of wound rotor synchronous machine using subharmonic excitation for brushless operation," *Energies*, vol. 11, no. 3, p. 554, Mar. 2018.

[27] M. Ayub, A. Hussain, G. Jawad, and B.-I. Kwon, "Brushless operation of a wound-field synchronous machine using a novel winding scheme," *IEEE Trans. Magn.*, vol. 55, no. 6, pp. 1–4, Jun. 2019, doi: 10.1109/TMAG.2019.2893883.

[28] A. Hussain, S. Atiq, and B.-I. Kwon, "Consequent-pole hybrid brushless wound-rotor synchronous machine," *IEEE Trans. Magn.*, vol. 54, no. 11, pp. 1–5, Nov. 2018, doi: 10.1109/TMAG.2018.2837690.

[29] M. Ayub, G. Jawad, and B.-I. Kwon, "Consequent-pole hybrid excitation brushless wound field synchronous machine with fractional slot concentrated winding," *IEEE Trans. Magn.*, vol. 55, no. 7, pp. 1–5, Jul. 2019, doi: 10.1109/TMAG.2018.2890509.

[30] J. G. Vaidya, M. L. Bansal, and H. Mansir, "Multiple output decoupled synchronous generator and electrical system employing same," U.S. Patent 5 764 036, Jun. 9, 1998.

[31] C. Chakraborty and Y. T. Rao, "Performance of brushless induction excited synchronous generator," *IEEE J. Emerg. Sel. Topics Power Electron.*, vol. 7, no. 4, pp. 2571–2582, Dec. 2019, doi: 10.1109/JESTPE.2018.2881068.

MUHAMMAD AYUB was born in Quetta, Pakistan. He received the B.S. degree from the Balochistan University of Information Technology, Engineering, and Management Sciences (BUITEMS), Quetta, in 2008. He is currently pursuing the Ph.D. degree with the Department of Electrical and Electronic Engineering, Hanyang University, Ansan, South Korea. He was worked in the capacity of Lecturer with BUITEMS. His research interest includes electric machine design and control.

SHAHID ATIQ was born in Punjab, Pakistan. He received the bachelor's and master's degrees from the University of Engineering and Technology Taxila, Pakistan, and the Ph.D. degree from Energy Conversion Systems Laboratory, Hanyang University, South Korea. He held different managerial and educational posts at various institutions. He is currently serving as an Associate Professor and the Head of the Department of Electrical Engineering, Khwaja Fareed University of Engineering and Information technology, Rahim Yar Khan, Pakistan.

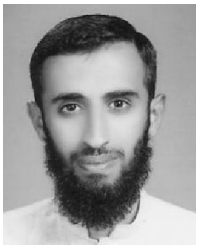

QASIM ALI was born in Abbottabad, Pakistan, in 1989. He received the B.S. degree in electronic engineering from COMSATS University Islamabad, Abbottabad Campus, Pakistan, in 2013, and the Ph.D. degree from Energy Conversion Systems Laboratory, Hanyang University, South Korea, in August 2018. He is currently working as an Assistant Professor with the Department of Electrical Engineering, Sukkur IBA, Sindh, Pakistan. His research interest includes electric machine design and control.

ASIF HUSSAIN was born in Quetta, Pakistan. He received the B.Sc. degree in electrical engineering from BZU, Multan, Pakistan, in 2005, and the Ph.D. degree from the Energy Conversion Systems Laboratory, Hanyang University, South Korea, in 2018. He is currently working as an Assistant Professor with the Department of Electrical Engineering, University of Management and Technology, Lahore, Pakistan. His research interest includes wound rotor synchronous machine design and control.

BYUNG-IL KWON (Senior Member, IEEE) was born in 1956. He received the B.S. and M.S. degrees in electrical engineering from Hanyang University, Ansan, South Korea, in 1981 and 1983, respectively, and the Ph.D. degree in electrical engineering, machine analysis from the University of Tokyo, Tokyo, Japan, in 1989. From 1989 to 2000, he was a Visiting Researcher with the Faculty of Science and Engineering Laboratory, University of Waseda, Tokyo, Japan. In 1990, he was a Researcher with the Toshiba System Laboratory, Yokohama, Japan. In 1991, he was a Senior Researcher with the Institute of Machinery and Materials Magnetic Train Business, Daejeon, South Korea. From 2001 to 2008, he was a Visiting Professor with the University of Wisconsin–Madison, Madison, WI, USA. He is currently a Professor with Hanyang University. His research interest includes design and control of electric machines.